Angular Dependence of Stimulated Brillouin Scattering in Homogeneous Plasma

Stimulated Brillouin scattering (SBS)[1] is the decay of an incident, or pump, light wave (0) into a frequency-downshifted, or Stokes, light wave (1) and an ion-acoustic wave (2). The conservation of energy and momentum in this process is reflected in the frequency and wave-vector matching conditions

$$\omega_0 = \omega_1 + \omega_2, \quad \mathbf{k}_0 = \mathbf{k}_1 + \mathbf{k}_2, \tag{1}$$

the second of which is illustrated in Fig. 60.13(a). For future reference, notice that the ion-acoustic wave number k_2 is maximal for directly backward scatterering and is equal to zero for directly forward scattering.

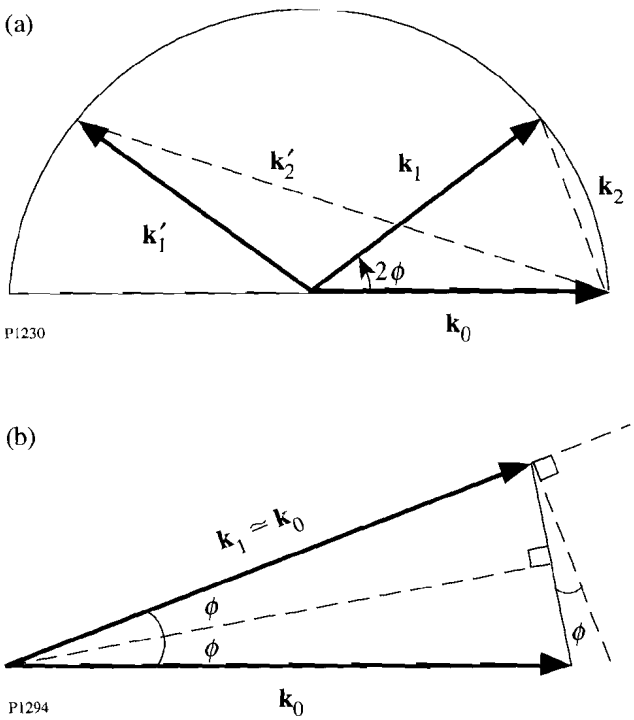

Figure 60.13
Interaction geometry for SBS. The angular dependence of γ_0, the temporal growth rate of SBS, stems from the fact that $k_2 \approx 2k_0 \sin\phi$.

SBS is important in the field of inertial confinement fusion (ICF)[2] because it can scatter the incident light away from the target, thereby reducing the amount of energy available to drive the compressive heating of the nuclear fuel. ICF experiments have involved plasmas with density and temperature scale lengths shorter than 100 μm for much of the last two decades, and analyses of parametric instabilities such as SBS have focused on the effects of these plasma inhomogeneities.[3] However, current experiments are designed to produce plasma conditions relevant to the proposed National Ignition Facility and involve plasmas with millimeter scale lengths. There has been a resurgence of interest in the predictions of the simpler homogeneous-plasma model because such long scale lengths diminish the importance of the effects of plasma inhomogeneities.

Traditionally, analyses of SBS begin with the determination of γ_0, the temporal growth rate of SBS in an infinite homogeneous plasma. It is well known that γ_0 is maximal for directly backward scattering and is equal to zero for directly forward scattering.[1] Physically, this behavior occurs because the ponderomotive force that drives the ion-acoustic wave is proportional to the square of the ion-acoustic wave number. Recognition of this behavior has led to the commonly held belief that backward SBS should dominate experiments involving long-scale-length plasmas.

The problem with this conclusion is that SBS cannot grow exponentially in time, with growth rate γ_0, for a time longer than that taken for light to cross the interaction region.[4] In current experiments, this transit time does not exceed a few picoseconds. In contrast, the temporal pulsewidth of a typical laser is a few nanoseconds, and the initial period of temporal growth is followed by a much longer period of spatiotemporal growth. If the incident laser intensity is less than the threshold intensity for the absolute instability, SBS will eventually saturate due to the convection of the Stokes and ion-acoustic waves out of the interaction region. If this convective saturation occurs on a nanosecond time scale, the angular dependence of the scattered light will be determined predominantly

by the physics of steady-state amplification. The goal of the work presented in this article is to determine how the convective amplification of the Stokes wave depends on the scattering angle and the conditions under which a steady-state analysis is applicable.

Governing Equations

The starting point for this investigation is Maxwell's wave equation

$$\left(\partial_{tt}^2 + \omega_e^2 - c^2\nabla^2\right)\mathbf{A}_h = -\omega_e^2 n_l \mathbf{A}_h \tag{2}$$

for the vector potential, together with the ion-acoustic wave equation

$$\left(\partial_{tt}^2 - c_s^2\nabla^2\right)n_l = \frac{1}{2}c_s^2\nabla^2\left\langle \mathbf{A}_h \cdot \mathbf{A}_h \right\rangle. \tag{3}$$

These equations were derived[5,6] under the assumption that the backgound plasma is uniform and at rest. The vector potential is normalized in such a way that $\mathbf{A}_h$ represents the velocity of electrons oscillating in the high-frequency electric field divided by a characteristic speed that is approximately equal to the electron thermal speed and n_l represents the low-frequency electron-density fluctuation associated with the ion-acoustic wave divided by the background elecron density. The symbol ω_e denotes the electron plasma frequency,[6] and the symbol c_s denotes the ion-acoustic speed.[7] Only the low-frequency plasma response to the ponderomotive force was retained, as is signified by the $\langle\ \rangle$ in Eq. (3).

SBS involves the interaction of two light waves and an ion-acoustic wave. These waves are coupled because of the electron current and the ponderomotive force, both of which are nonlinear. Because the effects of this coupling manifest themselves as slow spatial and temporal modulations of the wave amplitudes, the vector potential is written as

$$\begin{aligned}\mathbf{A}_h(\mathbf{r},t) = \mathbf{z}\Big\{&A_0\exp\left[i\left(\mathbf{k}_0\cdot\mathbf{r}-\omega_0 t\right)\right]\\ &+A_1(x,y,t)\exp\left[i\left(\mathbf{k}_1\cdot\mathbf{r}-\omega_1 t\right)\right]\Big\},\end{aligned} \tag{4}$$

where $\mathbf{k}_0$ and $\mathbf{k}_1$ are parallel to the xy plane, $(\omega_0,\mathbf{k}_0)$ and $(\omega_1,\mathbf{k}_1)$ satisfy the dispersion relation $\omega^2 = \omega_e^2 + c^2k^2$, and

$$\nabla A_1 \ll \mathbf{k}_1 A_1,\ \partial_t A_1 \ll \omega_1 A_1. \tag{5}$$

In this linearized analysis of the initial evolution of SBS, the amplitude of the incident wave is held fixed. The electron-density fluctuation is written as

$$n_l(\mathbf{r},t) = A_2(x,y,t)\exp\left[i\left(\mathbf{k}_2\cdot\mathbf{r}-\omega_2 t\right)\right], \tag{6}$$

where $\omega_2 = c_s k_2$ and A_2 satisfies an equation similar to Eq. (5). By substituting Ansaetze (4) and (6) into Eqs. (2) and (3), and collecting terms of like frequency and wave vector, one finds that

$$\begin{aligned}\left(\partial_t + \mathbf{v}_1\cdot\nabla + \nu_1\right)B_1 &= \gamma_0 B_2,\\ \left(\partial_t + \mathbf{v}_2\cdot\nabla + \nu_2\right)B_2 &= \gamma_0 B_1.\end{aligned} \tag{7}$$

In Eqs. (7) the dependent variables

$$B_1 = \omega_1^{1/2}A_1,\quad B_2 = -i\omega_e A_2^*/\omega_2^{1/2} \tag{8}$$

are proportional to the action amplitudes of the Stokes and ion-acoustic waves, respectively, and the group velocities

$$\mathbf{v}_1 = c^2\mathbf{k}_1/\omega_1,\quad \mathbf{v}_2 = c_s\mathbf{k}_2/k_2. \tag{9}$$

Phenomenological damping terms were added to each wave equation. The Stokes wave is damped by electron-ion collisions[6] and

$$\nu_1 = \omega_e^2\nu_{ei}/2\omega_1^2. \tag{10}$$

For plasmas in which $(T_i/m_i)^{1/2} \ll \omega_2/k_2 \ll (T_e/m_e)^{1/2}$, the Landau contribution to the ion-acoustic damping rate[7] is given by

$$\frac{\nu_2}{c_s k_2} \approx \left(\frac{\pi}{8}\right)^{1/2}\left[\left(\frac{ZT_e}{T_i}\right)^{3/2}\exp\left(-\frac{ZT_e}{2T_i}-\frac{3}{2}\right)+\left(\frac{Zm_e}{m_i}\right)^{1/2}\right]. \tag{11}$$

Relation (11) is based on the assumption that the ion-acoustic wavelength is much longer than the electron Debye length, an assumption that is also inherent in Eq. (3). The coupling parameter

$$\gamma_0 = \frac{\omega_e c_s k_2 A_0}{2(\omega_1 c_s k_2)^{1/2}}, \tag{12}$$

where the peak amplitude of the incident wave is given by the convenient formula

$$2A_0 \approx \frac{1.9\times10^{-8}\left[I(\mathrm{W/cm^2})\right]^{1/2}\lambda_0(\mu\mathrm{m})}{\left[T_e(\mathrm{keV})\right]^{1/2}\left[1+3(T_i/ZT_e)\right]^{1/2}}. \tag{13}$$

It is clear from Fig. 60.13(b) that $k_2 \approx 2k_0 \sin\phi$. Thus, one can exhibit the angular dependence of the coupling parameter and the ion-acoustic damping rate by writing

$$\gamma_0(\phi) = \gamma_b(\sin\phi)^{1/2}, \quad v_2(\phi) = v_b \sin\phi, \tag{14}$$

where the subscript b denotes values appropriate for backward SBS. In a similar vein,

$$v_{2x} = -c_s \sin\phi. \tag{15}$$

Steady-State Amplification of the Stokes Wave

In experiments typical of ICF the growth of the Stokes wave is initiated within the plasma by ion-acoustic fluctuations. This process is referred to in the nonlinear optics literature as Stokes generation and has been analyzed by Boyd, Rzazewski, and Narum.[8] By neglecting the convection of the acoustic wave, they showed that the time-asymptotic Stokes output can be written as the product of two terms: a source factor that depends on the amplitude of the acoustic fluctuations and an exponential gain factor that does not depend on the amplitude of the acoustic fluctuations. Furthermore, the exponent of the gain factor is identical to that for the Stokes amplification process, in which an externally generated Stokes wave is amplified convectively as it propagates through the medium. A preliminary analysis of Stokes generation in a plasma, which includes the convection of the ion-acoustic wave, has been made by McKinstrie *et al.*[9] The inclusion of ion-acoustic wave convection allows SBS to be absolutely unstable when the laser intensity is sufficiently high. However, in the convectively unstable regime, the Stokes output tends to a time-asymptotic steady state, and the gain exponents for Stokes generation and Stokes amplification are identical, as one should expect. Thus, one can avoid the mathematical difficulties associated with the analysis of Stokes generation and still obtain useful information regarding the angular dependence of SBS by analyzing Stokes amplification in the convectively unstable regime.

The interaction geometry for Stokes amplification is shown in Fig. 60.14(a). Initially,

$$B_1(x,y,0) = 0, \quad B_2(x,y,0) = 0. \tag{16}$$

At time $t = 0$ the leading edge of the externally generated Stokes wave enters the plasma with unit amplitude and initiates the instability. The ion-acoustic wave has zero amplitude at its entrance boundaries. For simplicity, we assume that the plasma is square and that its boundaries are aligned with the x and y axes. Thus, for $t > 0$,

$$B_1(0,y,t) = 1, \quad B_2(x,0,t) = 0, \quad B_2(l,y,t) = 0. \tag{17}$$

For a plasma with sides of length 100 μm, the transit time of the Stokes wave is 0.3 ps. In contrast, the transit time of the ion-acoustic wave is of the order of $7(m_i/m_e)^{1/2}$ ps for an electron temperature of 1 keV. Since the duration of a typical laser pulse is of the order of 1 ns, the information that a side boundary is present at $y = 0$ will not reach the plasma interior until the later stages of a typical experiment. Since the amplitude of the Stokes wave at its entrance boundary is independent of y, the initial evolution of SBS in the plasma interior is approximately one-dimensional and is governed approximately

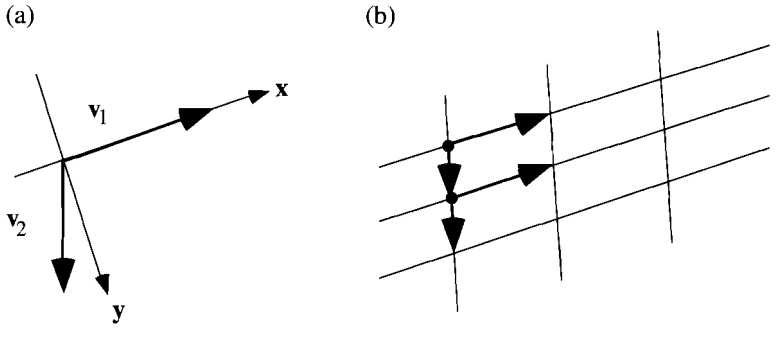

Figure 60.14
Group-velocity geometry for SBS. (a) The x component of $\mathbf{v}_2$ is always negative. (b) The initial evolution of SBS is approximately one-dimensional because the convection of portions of the ion-acoustic wave away from a particular Stokes ray is compensated by the convection of neighboring portions of the ion-acoustic wave toward that Stokes ray.

by the equations

$$\left(\partial_t + v_{1x}\partial_x + \nu_1\right)B_1 = \gamma_0 B_2\,,$$
$$\left(\partial_t - v_{2x}\partial_x + \nu_2\right)B_2 = \gamma_0 B_1\,, \tag{18}$$

where v_{2x} is defined to be positive.

Physically, this simplification occurs because the convection of portions of the ion-acoustic wave away from a particular Stokes ray is compensated by the convection of neighboring portions of the ion-acoustic wave toward that Stokes ray, as shown in Fig. 60.14(b). Notice that the preceding argument did not depend sensitively on the shape or alignment of the plasma.

The consequences of the one-dimensional model [Eqs. (18)] will now be studied, under the assumption that the instability grows and saturates convectively in a time that is short compared to the duration of the laser pulse. In steady state, the boundary conditions are

$$B_1(0) = 1, \quad B_2(l) = 0. \tag{19}$$

It is not difficult to show that

$$B_1(x) = \frac{\left\{\beta\cosh\left[\beta(l-x)\right] + \alpha_s \sinh\left[\beta(l-x)\right]\right\}\exp(\alpha_d x)}{\left[\beta\cosh(\beta l) + \alpha_s \sinh(\beta l)\right]},$$
$$B_2(x) = \frac{\gamma_0 \sinh\left[\beta(l-x)\right]\exp(\alpha_d x)}{v_{2x}\left[\beta\cosh(\beta l) + \alpha_s \sinh(\beta l)\right]}, \tag{20}$$

where the auxiliary parameters

$$\alpha_1 = \nu_1/v_{1x}\,, \quad \alpha_2 = \nu_2/v_{2x}\,,$$
$$\alpha_s = (\alpha_2 + \alpha_1)/2, \quad \alpha_d = (\alpha_2 - \alpha_1)/2, \tag{21}$$

and

$$\beta = \left(\alpha_s^2 - \gamma^2\right)^{1/2}, \quad \gamma = \gamma_0/\left(v_{1x}v_{2x}\right)^{1/2}. \tag{22}$$

The wave amplitudes $B_1(x)$ and $\left(v_{2x}/v_{1x}\right)^{1/2} B_2(x)$ are plotted in Fig. 60.15 for the case in which $\alpha_1 l = 0$, $\alpha_2 l = 52$, and $\gamma l = 17$. These parameters, which are used throughout most of this article, correspond to a singly ionized plasma with a background electron density of $10^{19}/\text{cm}^3$, an electron temperature of 1 keV, an ion temperature of 0.1 keV and a length of 100 μm, and a laser intensity of 5×10^{14} W/cm^2.

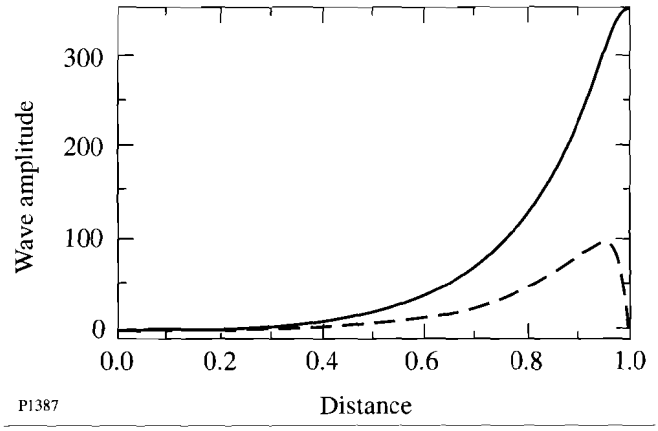

Figure 60.15
Steady-state amplitudes of the Stokes (solid line) and ion-acoustic (broken line) waves [Eqs. (20)] plotted as functions of distance for the case in which the damping parameters $\alpha_1 l = 0$ and $\alpha_2 l = 52$, and the pump-strength parameter $\gamma l = 17$. These parameters are all independent of the scattering angle 2ϕ. Distance is measured in units of the plasma length l.

It follows from the first of Eqs. (20) that the convective gain associated with the Stokes amplification process, which is defined as $B_1(l)/B_1(0)$, is given by[10]

$$G = \frac{\beta\exp(\alpha_d l)}{\beta\cosh(\beta l) + \alpha_s \sinh(\beta l)}. \tag{23}$$

It follows from Eqs. (14), (21), and (22) that the auxiliary parameters used in Eq. (23) are all independent of the scattering angle 2ϕ. This fact has two important consequences.

First, although γ_0, the temporal growth rate of SBS, is proportional to $(\sin\phi)^{1/2}$, the steady-state convective gain associated with this one-dimensional model of Stokes amplification is independent of the scattering angle.[11] Typically, $\alpha_1 \ll \alpha_2$. When $\beta l \ll 1$ one can write

$$G \propto \exp(gl), \tag{24}$$

where the spatial growth rate

$$g \approx \frac{v_b}{2v_2} - \left[\left(\frac{v_b}{2v_2}\right)^2 - \frac{\gamma_b^2}{v_1 v_2}\right]^{1/2}. \tag{25}$$

In typical nonlinear optics experiments the low acoustic speed results in strong spatial damping of the acoustic wave and

$$g \approx \gamma_b^2 / v_1 \nu_b . \tag{26}$$

Equation (26) is independent of the acoustic speed, as one should expect. The exact and approximate gain exponents [Eqs. (25) and (26)] are plotted as functions of the pump-intensity parameter $(\gamma l)^2$ in Fig. 60.16 for the case in which $\alpha_2 l$ = 52. For a pump-intensity parameter of 600, which corresponds to a laser intensity of approximately 10^{15} W/cm^2, use of the approximate gain exponent leads to an estimate of the intensity of the Stokes output that is five orders of magnitude too low! This result shows the importance of retaining the effects of ion-acoustic wave convection in analyses of SBS in plasmas.[9]

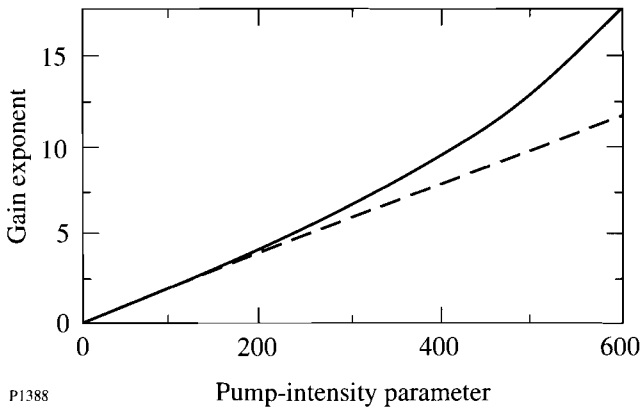

Figure 60.16
Exact (solid line) and approximate (broken line) gain exponents of SBS [Eqs. (25) and (26)] plotted as functions of the pump-intensity parameter $(\gamma l)^2$ for the case in which $\alpha_1 l = 0$ and $\alpha_2 l = 52$. The large discrepancy between the gain exponents demonstrates the importance of ion-acoustic wave convection. This result distinguishes plasmas from most other nonlinear optical media.

It is well known that the steady-state convective gain becomes infinite when the denominator of Eq. (23) vanishes. This singularity can occur when $\gamma > \alpha_2/2$ and signifies the onset of absolute instability. The second important consequence of the fact described after Eq. (23) is that, in the context of this one-dimensional model, the absolute instability condition for SBS is independent of the scattering angle.[11] Physically, the existence of absolute instability stems from the fact that the component of the ion-acoustic velocity in the direction of the Stokes velocity is always negative [Eq. (15)].

The results described in the preceding two paragraphs are in apparent contradiction to the well known fact that $\gamma_0 \to 0$ as $\phi \to 0$ and, hence, that directly forward SBS does not exist. One can resolve this apparent contradition by realizing that the response of the acoustic wave to the ponderomotive force of the pump and Stokes waves is like that of a driven harmonic oscillator, in which the oscillator takes several damping times to attain its steady-state response. Since v_2 is proportional to $\sin\phi$, the saturation time associated with this one-dimensional model of SBS tends to infinity as the scattering angle tends to zero, and use of the steady-state gain formula is inappropriate in this limit.

Transient Evolution of SBS

The exact solutions of Eqs. (18) have been obtained for a finite plasma by Bobroff and Haus[12] and by Williams and McGowan.[13] However, these solutions are written in terms of infinite sums of modified Bessel functions, and, because of their complexity, a different approach is taken here. Since the duration of a typical laser pulse is comparable to the transit time of the acoustic wave, one might suspect that the initial evolution of SBS does not depend sensitively on the finite-plasma boundary conditions. In this vein, consider the evolution of SBS in an infinite plasma. The arrival of an externally generated Stokes wave at $x = 0$ is modeled by adding a source term

$$S_1(x,t) = v_{1x}\delta(x)H(t) \tag{27}$$

to the first of Eqs. (18). The corresponding temporal growth and saturation of the Stokes output $B_1(l,t)$ will be studied analytically. The results obtained from this approximate analysis will then be verified by solving Eqs. (18) numerically for a finite plasma.

It is shown in the Appendix that, consistent with Eq. (27), the Stokes wave evolves according to

$$B_1(x,t) = v_{1x}\int_0^t G_{11}(x,t')dt', \tag{28}$$

where

$$
\begin{aligned}
G_{11}(x,t) &= \frac{\gamma_0}{v_{1x}+v_{2x}}\left(\frac{x+v_{2x}t}{v_{1x}t-x}\right)^{1/2} \\
&\times I_1\left(\frac{2\gamma_0\left[(x+v_{2x}t)(v_{1x}t-x)\right]^{1/2}}{v_{1x}+v_{2x}}\right) \\
&\times \exp\left[-\frac{\nu_1(x+v_{2x}t)}{v_{1x}+v_{2x}}-\frac{\nu_2(v_{1x}t-x)}{v_{1x}+v_{2x}}\right] \\
&\times H(x+v_{2x}t)H(v_{1x}t-x) \\
&+ H(x+v_{2x}t)\delta(v_{1x}t-x)\exp(-\nu_1 t) \qquad (29)
\end{aligned}
$$

is the Green function that describes the effect on the Stokes wave at the point (x,t) of an impulse applied to it at the point (0,0). The impulse response $G_{11}(l,t)$ is displayed in Fig. 60.17 for the case in which $\alpha_1 l = 0$, $\alpha_2 l = 52$, and $\gamma l = 17$. The impulse response grows in time until it attains its maximal amplitude at $t = t_*$. Subsequently, it decays in a time comparable to the growth time. Since the time-asymptotic Stokes output is proportional to the area under the impulse response curve [Eq. (28)], it is reasonable to define the saturation time t_s as $2t_*$. Using the fact that

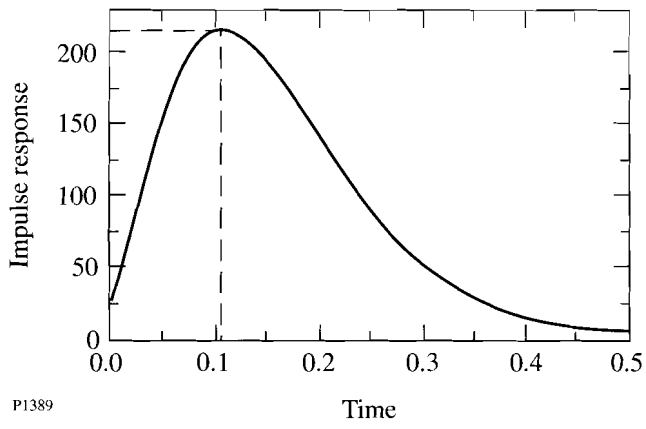

Figure 60.17
Impulse response of the Stokes wave at its exit boundary $x = l$ [Eqs. (28) and (29)] plotted as a function of time for the case in which $\alpha_1 l = 0$, $\alpha_2 l = 52$, and $\gamma l = 17$. Time is measured in units of the ion-acoustic transit time l/v_{2x}.

$$I_1(z) \sim \exp(z)/(2\pi z)^{1/2} \qquad (30)$$

as $z \to \infty$, one can see that

$$
\begin{aligned}
G_{11}(x,t) \propto \exp\Bigg(&\frac{2\gamma_0\left[(x+v_{2x}t)(v_{1x}t-x)\right]^{1/2}}{v_{1x}+v_{2x}} \\
&-\frac{\nu_1(x+v_{2x}t)}{v_{1x}+v_{2x}}-\frac{\nu_2(v_{1x}t-x)}{v_{1x}+v_{2x}}\Bigg) \qquad (31)
\end{aligned}
$$

for large values of t. Let $\psi(x,t)$ be the exponent in Eq. (31). Then t_*, the time of maximal growth, is found from the condition

$$\partial_t\left[\psi(l,t)\right]_{t_*} = 0. \qquad (32)$$

It is not difficult to show that

$$t_* = \frac{(\xi_2+\xi_1)\alpha_s-(\xi_2-\xi_1)\left(\alpha_s^2-\gamma^2\right)^{1/2}}{2\left(\alpha_s^2-\gamma^2\right)^{1/2}}, \qquad (33)$$

where

$$\xi_1 = l/v_{1x}, \quad \xi_2 = l/v_{2x}. \qquad (34)$$

It can also be shown that

$$B_1(l,t_*) \propto \exp\left[(\alpha_d-\beta)l\right], \qquad (35)$$

in keeping with Eqs. (23)–(25).

The preceding analysis is consistent with previous analyses in the plasma physics literature,[4] in which Fourier analysis was used to determine the impulse response function $\gamma(v_x)$, defined as the time-asymptotic temporal growth rate of the portion of the impulse response that convects with x velocity v_x. It follows from Eq. (31) that

$$\lim_{t\to\infty} G_{11}(v_x t,t) \propto \exp\left[\gamma(v_x)t\right], \qquad (36)$$

where

$$\gamma(v_x) = \frac{2\gamma_0\left[(v_x + v_{2x})(v_{1x} - v_x)\right]^{1/2}}{v_{1x} + v_{2x}} - \frac{\nu_1(v_x + v_{2x})}{v_{1x} + v_{2x}} - \frac{\nu_2(v_{1x} - v_x)}{v_{1x} + v_{2x}}. \quad (37)$$

The impulse response function $\gamma(v_x)$ is displayed in Fig. 60.18. Consider the portion of the impulse response that convects with velocity v_x. This portion of the impulse response travels a distance l in a time l/v_x, at which point it has grown by a factor proportional to $\exp\left[\gamma(v_x)l/v_x\right]$. Thus, $\gamma(v_x)/v_x$ is the spatial growth rate of this portion of the impulse response. In the figure this spatial growth rate is the slope of a straight line from the origin to the point $\left(v_x, \gamma(v_x)\right)$ on the impulse response curve. It follows from the figure that the amplitude of the impulse response at $x = l$ increases with time until $t_* = l/v_*$, where v_*, the velocity of maximal spatial gain, is found from the condition

$$\frac{d}{dv_x}\left[\frac{\gamma(v_x)}{v_x}\right]_{v_*} = 0. \quad (38)$$

Subsequently, the amplitude of the impulse response decreases with time. It is clear physically that definition (38) is identical to definition (32). To establish their equivalence mathematically, one need only observe that, with x fixed,

$$\frac{d}{dv_x}\left[\frac{\gamma(v_x)}{v_x}\right] = \frac{d}{d(x/t)}\left[\frac{\gamma(x/t)t}{x}\right] = -\frac{t^2}{x^2}\frac{\partial\psi}{\partial t}. \quad (39)$$

Since $v_2 \ll v_1$, $\xi_1 \ll \xi_2$ for all scattering angles, and it follows from Eqs. (15) and (33) that t_s is proportional to $l/\sin\phi$.[11] This result verifies the statement that the saturation time tends to infinity as the scattering angle tends to zero. The angular dependence of the saturation time is displayed in Fig. 60.19(a). For a scattering angle of 30°, the saturation time is longer than that for directly backward scattering by a factor of approximately 4. For a scattering angle of 10°, this factor is approximately equal to 11. Typically, $\alpha_1 \ll \alpha_2$, and it follows from Eq. (33) that

$$\frac{v_{2x}t_s}{l} \approx \frac{\alpha_2 - \left(\alpha_2^2 - 4\gamma^2\right)^{1/2}}{\left(\alpha_2^2 - 4\gamma^2\right)^{1/2}}. \quad (40)$$

The coefficient of the saturation time appearing on the right side of Eq. (40) is independent of the plasma length and the scattering angle. It is plotted as a function of γl in Fig. 60.19(b) for the case in which $\alpha_2 l = 52$. Provided that the value of γ is not too close to its absolute threshold value of $\alpha_2/2$, the saturation time is much less than the transit time of the ion-acoustic wave, and our use of the infinite-medium Green function seems reasonable. As a further check of the validity of this approximation, Eqs. (18) were solved numerically for a finite plasma by a computer code based on the method of characteristics. The numerically determined Stokes output is plotted as a function of time in Fig. 60.20 for the case in which $\alpha_2 l = 52$ and $\gamma l = 17$. The saturation time of 0.30 l/v_{2x} predicted by Eq. (40) is consistent with the numerically determined Stokes output displayed in Fig. 60.20. The coefficient of the saturation time is also plotted as a function of the electron density and temperature in Figs. 60.21(a) and 60.21(b), respectively. The assumption that backward SBS grows and saturates convectively in a time that is short compared to the duration of the laser pulse is valid for the parameters chosen to illustrate the results of this article. [See the description of Fig. 60.15 that follows Eq. (22).] However, if the plasma length, the background electron density, or the laser intensity is significantly longer, or higher, than the value chosen for this article, or the electron temperature is significantly lower, backward SBS does not saturate and the steady-state results of the section on steady-state amplification do not apply. In this

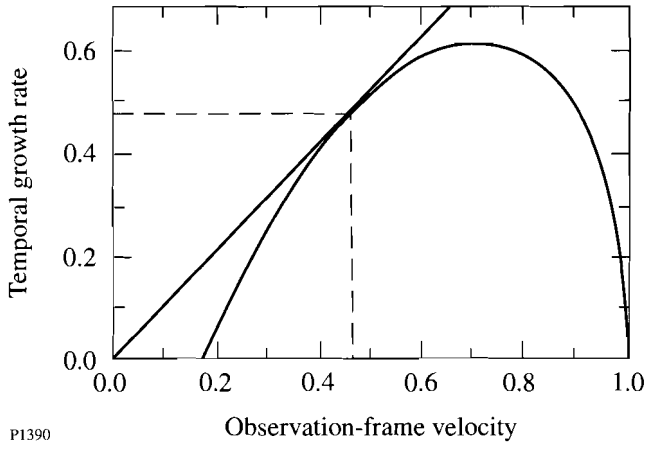

Figure 60.18
Sketch of the apparent temporal growth rate of the impulse response of the Stokes wave [Eq. (37)]. The temporal growth rate is measured in units of γ_0, and the observation-frame velocity is measured in units of v_{1x}.

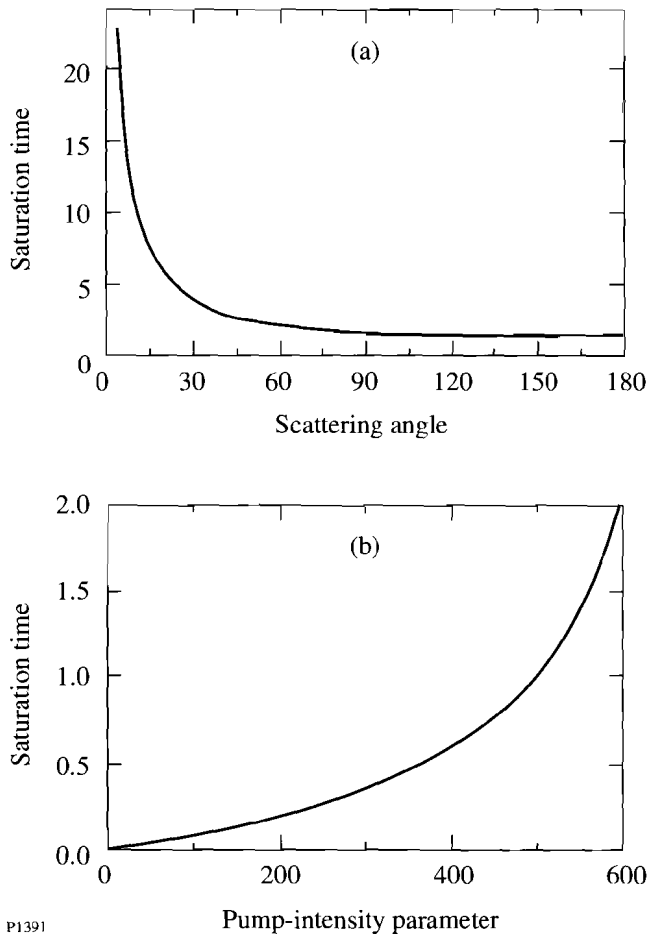

Figure 60.19
Characteristics of the convective saturation time of SBS [Eq. (40)]. (a) The saturation time, normalized to the saturation time of backward SBS, is plotted as a function of the scattering angle 2ϕ. (b) The saturation time of backward SBS, normalized to the transit time of the ion-acoustic wave, is plotted as a function of the pump-intensity parameter $(\gamma l)^2$.

case, a detailed spatiotemporal analysis of SBS[12,13] is required. In the strong damping regime typical of nonlinear optics experiments, Eq. (40) reduces to

$$v_2 t_s \approx 2\gamma_b^2 l / v_1 v_b . \qquad (41)$$

The saturation time is still proportional to $l/\sin\phi$, as it must be, but is independent of the acoustic speed.

As discussed in the preceding paragraph, the saturation time associated with the one-dimensional model described herein tends to infinity as the scattering angle tends to zero. It is reasonable to conclude that, at any instant of time, the Stokes output decreases as the scattering angle decreases. However, a detailed spatiotemporal analysis of SBS in a finite plasma[12,13] is required to quantify the angular dependence of the Stokes output. Furthermore, as the scattering angle decreases and the one-dimensional saturation time increases, other saturation mechanisms for SBS become more important. In the context of linear theory, the only other saturation mechanism is the convection of the ion-acoustic wave in the y direction. McKinstrie *et al.*[14] have shown that this lateral convection of the ion-acoustic wave can saturate forward SBS on a time scale short compared to the one-dimensional saturation time and that the importance of lateral convection increases as the scattering angle decreases. However, as early saturation reduces the Stokes output, the general conclusion of this article—that the Stokes output decreases as the scattering angle decreases—is still correct.

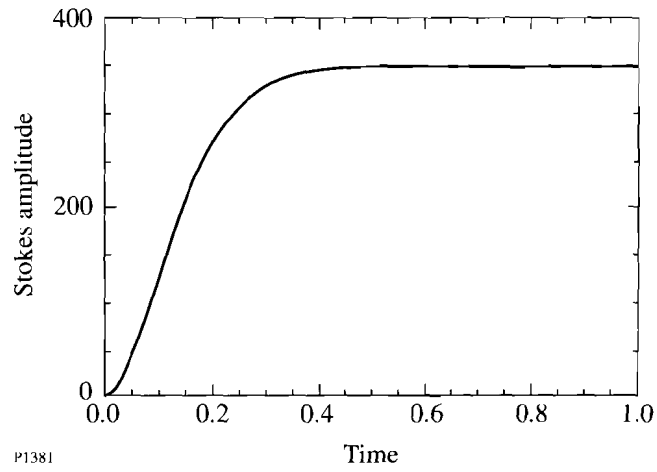

Figure 60.20
Stokes amplitude at $x = l$ plotted as a function of time for the case in which $\alpha_1 l = 0$, $\alpha_2 l = 52$, and $\gamma l = 17$. Time is measured in units of the ion-acoustic transit time. The evolution of the Stokes wave was determined by solving Eqs. (18) numerically for a finite plasma. The convective saturation time observed in this simulation is consistent with the prediction of Eq. (40).

Finally, it should be mentioned that numerical simulations of SBS in homogeneous plasma have been made by Amin *et al.*[15,16] for the complimentary case in which the ion-acoustic wave is subject to viscous damping. In principle, the preceding analysis applies also to this case; however, the second of Eqs. (14) should read $v_2 = v_b \sin^2\phi$. The consequences of this modified angular dependence for the one-dimensional model described herein are profound: First, forward SBS is absolutely unstable for arbitrary laser intensity. Second, even if the laser intensity is low enough that sideward and backward SBS are not absolutely unstable, the convective saturation time for

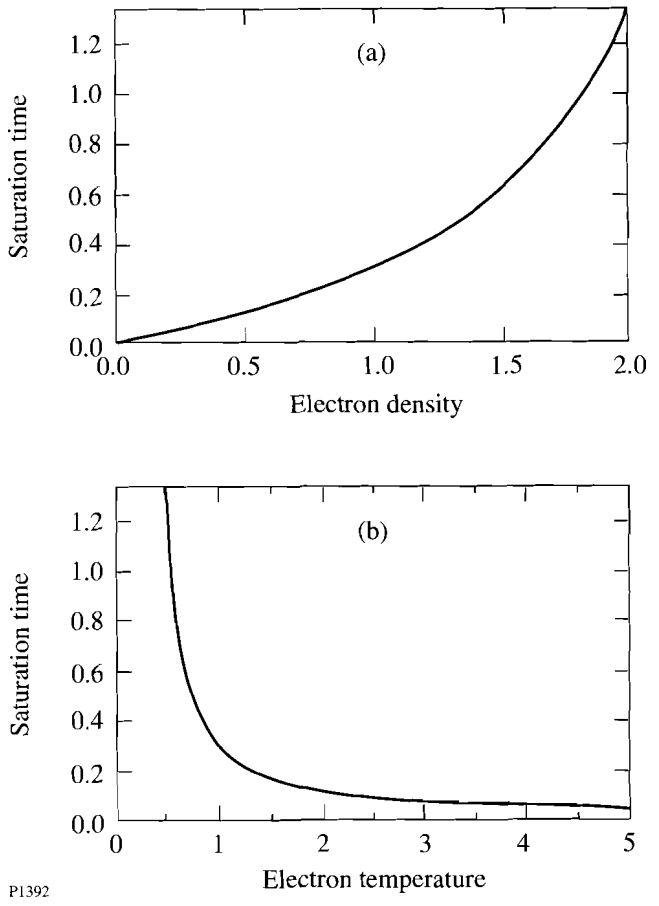

Figure 60.21
Characteristics of the convective saturation time of SBS [Eq. (40)]. (a) The saturation time, normalized to the transit time of the ion-acoustic wave, is plotted as a function of the background electron density, in units of $10^{19}/cm^3$, for an electron temperature of 1 keV. (b) The saturation time, normalized to the transit time of the ion-acoustic wave, is plotted as a function of the electron temperature, in keV, for a background electron density of $10^{19}/cm^3$. In both cases the ratio of the ion and electron temperatures is 0.1, and the laser intensity is 5×10^{14} W/cm^2.

sideward SBS is likely to be comparable to the temporal pulsewidth of the laser. In both cases a transient two-dimensional analysis of SBS[14] is required.

Summary

The angular dependence of stimulated Brillouin scattering (SBS) in a finite homogeneous plasma was studied. For parameters typical of current ICF experiments, the initial evolution of SBS is well approximated by a one-dimensional model. In the context of this model, the threshold intensity of the absolute instability and the steady-state spatial growth rate of the convective instability are both independent of the scattering angle. However, the saturation time of the convective instability exhibits a strong inverse dependence on the scattering angle: Forward SBS always occurs in the transient regime, and the intensity of the scattered light is less than that predicted by a steady-state analysis. In particular, no light is emitted in the direction parallel to the wave vector of the incident wave. Thus, the commonly held belief that backward SBS should dominate experiments involving long-scale-length plasmas is correct, but for reasons other than that on which it was originally based.

Finally, although the analysis of this article was directed at SBS, Eqs. (7) apply to other parametric instabilities such as stimulated Raman scattering (SRS). Thus, subject to the constraints described in the previous section, the main analytical results of this article should be valid for SRS.

ACKNOWLEDGMENT

This work was supported by the National Science Foundation under Contract No. PHY-9057093, the U. S. Department of Energy (DOE) Office of Inertial Confinement Fusion under Cooperative Agreement No. DE-FC03-92SF19460, the University of Rochester, and the New York State Energy Research and Development Authority. The support of DOE does not constitute an endorsement by DOE of the views expressed in this article.

Appendix: Green-Function Analysis of SBS in an Infinite Plasma

The wave amplitudes B_1 and B_2 defined in the section on governing equations evolve according to the equations

$$\begin{aligned}(\partial_t + v_1\partial_x + \nu_1)B_1 &= \gamma_0 B_2 + S_1(x,t),\\ (\partial_t - v_2\partial_x + \nu_2)B_2 &= \gamma_0 B_1 + S_2(x,t),\end{aligned} \tag{A1}$$

where S_1 and S_2 are phenomenological source terms that model the way in which SBS is initiated. Equations (A1) can be rewritten in the matrix form

$$LB = S, \tag{A2}$$

where

$$L = \begin{bmatrix}(\partial_t + v_1\partial_x + \nu_1) & -\gamma_0\\ -\gamma_0 & (\partial_t - v_2\partial_x + \nu_2)\end{bmatrix} \tag{A3}$$

and

$$B = \begin{bmatrix}B_1(x,t)\\ B_2(x,t)\end{bmatrix}, \quad S = \begin{bmatrix}S_1(x,t)\\ S_2(x,t)\end{bmatrix}. \tag{A4}$$

The Green matrix

$$G=\begin{bmatrix} G_{11}(x,t) & G_{12}(x,t) \\ G_{21}(x,t) & G_{22}(x,t) \end{bmatrix} \tag{A5}$$

satisfies the related equation

$$LG = D, \tag{A6}$$

where

$$D=\begin{bmatrix} \delta(x)\delta(t) & 0 \\ 0 & \delta(x)\delta(t) \end{bmatrix}. \tag{A7}$$

It is not difficult to verify that the solution of Eq. (A2) is

$$B(x,t)=\int_{-\infty}^{\infty}\int_{-\infty}^{\infty} G(x-x',t-t')S(x',t')dx'dt'. \tag{A8}$$

It follows from Eq. (A8) that the Green function $G_{ij}(x-x',t-t')$ describes the effect on wave i at the position (x,t) of an impulse applied to wave j at the position (x',t').

It is well known that the Green functions defined by Eqs. (A5)–(A7) can be written in terms of modified Bessel functions. However, as we are unaware of any derivation of this result published in the plasma physics literature, a simple derivation is included in this appendix for the benefit of the reader.

The determination of the Green matrix is facilitated by rewriting Eq. (A6) in terms of the characteristic variables

$$\xi = x + v_2 t, \quad \eta = v_1 t - x. \tag{A9}$$

By using these variables and the fact that

$$\delta(x)\delta(t) = \delta(\xi)\delta(\eta)J(\xi,\eta;x,t), \tag{A10}$$

where

$$J(\xi,\eta;x,t) = v_1 + v_2 \tag{A11}$$

is the Jacobian determinant associated with the transformation from (ξ,η) to (x,t), one can rewrite Eq. (A6) as

$$\begin{bmatrix} (\partial_\xi + \alpha_1) & -\gamma \\ -\gamma & (\partial_\eta + \alpha_2) \end{bmatrix}\begin{bmatrix} G_{11} & G_{12} \\ G_{21} & G_{22} \end{bmatrix}$$

$$=\begin{bmatrix} \delta(\xi)\delta(\eta) & 0 \\ 0 & \delta(\xi)\delta(\eta) \end{bmatrix}, \tag{A12}$$

where

$$\begin{aligned} \alpha_1 &= v_1/(v_1+v_2), \\ \alpha_2 &= v_2/(v_1+v_2), \\ \gamma &= \gamma_0/(v_1+v_2). \end{aligned} \tag{A13}$$

One can eliminate the damping terms α_1 and α_2 by defining

$$G(\xi,\eta) = \overline{G}(\xi,\eta)\exp(-\alpha_1\xi - \alpha_2\eta). \tag{A14}$$

The Green matrix $\overline{G}(\xi,\eta)$ satisfies the conservative equation

$$\begin{bmatrix} \partial_\xi & -\gamma \\ -\gamma & \partial_\eta \end{bmatrix}\begin{bmatrix} \overline{G}_{11} & \overline{G}_{12} \\ \overline{G}_{21} & \overline{G}_{22} \end{bmatrix}=\begin{bmatrix} \delta(\xi)\delta(\eta) & 0 \\ 0 & \delta(\xi)\delta(\eta) \end{bmatrix}, \tag{A15}$$

which is the simplest form of Eq. (A6).

The Green functions $\overline{G}_{11}(\xi,\eta)$ and $\overline{G}_{21}(\xi,\eta)$ satisfy the equations

$$\partial_\xi \overline{G}_{11} = \gamma\overline{G}_{21} + \delta(\xi)\delta(\eta), \quad \partial_\eta \overline{G}_{21} = \gamma\overline{G}_{11}. \tag{A16}$$

It follows from Eqs. (A16) and the theory of characteristics that $\overline{G}_{11}(\xi,\eta)$ and $\overline{G}_{21}(\xi,\eta)$ can only be nonzero for $\xi \geq 0$ and $\eta \geq 0$. In other words, one has to solve an initial value problem in the retarded time variable η on the half-space $\xi \geq 0$. A natural way to solve such a problem is by Laplace transforming in the variable η. It is not difficult to show that

$$\overline{G}_{21}(\xi,\eta) = \mathcal{L}^{-1}\left\{\frac{\gamma\exp(\gamma^2\xi/s)}{s}\right\}$$

$$=\gamma I_0\left[2\gamma(\xi\eta)^{1/2}\right]H(\xi)H(\eta). \tag{A17}$$

The Laplace transform tables of Abramowitz and Stegun[17] were used to invert the Laplace transform, and the Heaviside step functions $H(\xi)$ and $H(\eta)$ were added to ensure that the Green function equals zero for points outside the domain of influence of the source point. Similarly,

$$\bar{G}_{11}(\xi,\eta) = \mathcal{L}^{-1}\left\{ s\frac{\exp(\gamma^2\xi/s)}{s} - 1 + 1 \right\}$$

$$= \partial_\eta I_0\left[2\gamma(\xi\eta)^{1/2}\right] + \delta(\eta)$$

$$= \gamma(\xi/\eta)^{1/2} I_1\left[2\gamma(\xi\eta)^{1/2}\right] H(\xi)H(\eta) + H(\xi)\delta(\eta). \quad \text{(A18)}$$

Notice that $\bar{G}_{11}(\xi,\eta)$ is related to $\bar{G}_{21}(\xi,\eta)$ by the second of Eqs. (A16), as it must be. It follows from Eq. (A15) that $\bar{G}_{12}(\xi,\eta) = \bar{G}_{21}(\eta,\xi)$ and $\bar{G}_{22}(\xi,\eta) = \bar{G}_{11}(\eta,\xi)$.

In terms of the original variables x and t, the conservative Green functions are

$$\bar{G}_{11}(x,t) = \frac{\gamma_0}{v_1+v_2}\left(\frac{x+v_2t}{v_1t-x}\right)^{1/2} I_1\left(\frac{2\gamma_0\left[(x+v_2t)(v_1t-x)\right]^{1/2}}{v_1+v_2}\right)$$

$$\times H(x+v_2t)H(v_1t-x) + H(x+v_2t)\delta(v_1t-x),$$

$$\bar{G}_{12}(x,t) = \bar{G}_{21}(x,t) = \frac{\gamma_0}{v_1+v_2} I_0\left(\frac{2\gamma_0\left[(x+v_2t)(v_1t-x)\right]^{1/2}}{v_1+v_2}\right)$$

$$\times H(x+v_2t)H(v_1t-x), \quad \text{(A19)}$$

$$\bar{G}_{22}(x,t) = \frac{\gamma_0}{v_1+v_2}\left(\frac{v_1t-x}{x+v_2t}\right)^{1/2} I_1\left(\frac{2\gamma_0\left[(x+v_2t)(v_1t-x)\right]^{1/2}}{v_1+v_2}\right)$$

$$\times H(x+v_2t)H(v_1t-x) + \delta(x+v_2t)H(v_1t-x).$$

According to Eq. (A14), the dissipative Green functions are related to the conservative Green functions by

$$G_{ij}(x,t) = \bar{G}_{ij}(x,t)\exp\left[-\frac{v_1(x+v_2t)}{v_1+v_2} - \frac{v_2(v_1t-x)}{v_1+v_2}\right]. \quad \text{(A20)}$$

REFERENCES

1. J. F. Drake *et al.*, Phys. Fluids **17**, 778 (1974).
2. R. S. Craxton, R. L. McCrory, and J. M. Soures, Sci. Am. **255**, 68 (1986).
3. C. S. Liu, in *Advances in Plasma Physics*, edited by A. Simon and W. B. Thompson (Wiley, New York, 1976), Vol. 6, p. 121.
4. A. Bers, in *Basic Plasma Physics*, edited by A. A. Galeev and R. N. Sudan, Handbook of Plasma Physics (North Holland, Amsterdam, 1983), Vol. 1, p. 45 and references therein.
5. C. J. McKinstrie and M. V. Goldman, J. Opt. Soc. Am. B **9**, 1778 (1992).
6. W. L. Kruer, *The Physics of Laser Plasma Interactions*, Frontiers in Physics (Addison-Wesley, CA, 1988), Vol. 73, Chap. 8.
7. S. Ichimaru, *Basic Principles of Plasma Physics: A Statistical Approach*, Frontiers in Physics (Benjamin, Reading, MA, 1973), p. 71.
8. R. W. Boyd, K. Rzazewski, and P. Narum, Phys. Rev. A **42**, 5514 (1990).
9. C. J. McKinstrie, J. S. Li, R. Betti, and E. A. Williams, Paper 1O3, presented at the 23rd Annual Anomalous Conference, Wintergreen, VA, 21–25 June 1993. This work is being prepared for submittal to Physics of Plasmas.
10. C. J. McKinstrie and A. Simon, Phys. Fluids **29**, 1959 (1986) and references therein.
11. C. J. McKinstrie and R. E. Giacone, Bull. Am. Phys. Soc. **37**, 1440 (1992); R. E. Giacone, C. J. McKinstrie, R. Betti, and H. Chen, Bull. Am. Phys. Soc. **38**, 1914 (1993).
12. D. L. Bobroff and H. A. Haus, J. Appl. Phys. **38**, 390 (1967).
13. E. A. Williams and R. R. McGowan, in *Research Trends in Physics: Inertial Confinement Fusion*, edited by K. A. Brueckner (American Institute of Physics, New York, 1992), p. 325.
14. C. J. McKinstrie, R. Betti, R. E. Giacone, T. Kolber, and J. S. Li, Phys. Rev. E **50**, 2182 (1994).
15. M. R. Amin *et al.*, Phys. Rev. Lett. **71**, 81 (1993).
16. M. R. Amin *et al.*, Phys. Fluids B **5**, 3748 (1993).
17. M. Abramowitz and I. A. Stegun, eds., Handbook of Mathematical Functions (National Bureau of Standards, Washington, D.C., 1964), Chap. 29.